

Experimental validation of deterministic Acuros XB algorithm for IMRT and VMAT dose calculations with the Radiological Physics Center's head and neck phantom

Tao Han

Department of Radiation Physics, The University of Texas MD Anderson Cancer Center, Houston, Texas 77030

Firas Mourtada

Department of Radiation Physics, The University of Texas MD Anderson Cancer Center, Houston, Texas 77030 and Department of Radiation Oncology, Christiana Care Health System, Newark, Delaware 19713

Kelly Kisling, Justin Mikell, David Followill, and Rebecca Howell^{a)}

Department of Radiation Physics, The University of Texas MD Anderson Cancer Center, Houston, Texas 77030

(Received 31 October 2011; revised 9 January 2012; accepted for publication 14 February 2012; published 2 April 2012)

Purpose: The purpose of this study was to verify the dosimetric performance of Acuros XB (AXB), a grid-based Boltzmann solver, in intensity-modulated radiation therapy (IMRT) and volumetric-modulated arc therapy (VMAT).

Methods: The Radiological Physics Center (RPC) head and neck (H&N) phantom was used for all calculations and measurements in this study. Clinically equivalent IMRT and VMAT plans were created on the RPC H&N phantom in the Eclipse treatment planning system (version 10.0) by using RPC dose prescription specifications. The dose distributions were calculated with two different algorithms, AXB 11.0.03 and anisotropic analytical algorithm (AAA) 10.0.24. Two dose report modes of AXB were recorded: dose-to-medium in medium ($D_{m,m}$) and dose-to-water in medium ($D_{w,m}$). Each treatment plan was delivered to the RPC phantom three times for reproducibility by using a Varian Clinac iX linear accelerator. Absolute point dose and planar dose were measured with thermoluminescent dosimeters (TLDs) and GafChromic® EBT2 film, respectively. Profile comparison and 2D gamma analysis were used to quantify the agreement between the film measurements and the calculated dose distributions from both AXB and AAA. The computation times for AAA and AXB were also evaluated.

Results: Good agreement was observed between measured doses and those calculated with AAA or AXB. Both AAA and AXB calculated doses within 5% of TLD measurements in both the IMRT and VMAT plans. Results of AXB_ $D_{m,m}$ (0.1% to 3.6%) were slightly better than AAA (0.2% to 4.6%) or AXB_ $D_{w,m}$ (0.3% to 5.1%). The gamma analysis for both AAA and AXB met the RPC 7%/4 mm criteria (over 90% passed), whereas AXB_ $D_{m,m}$ met 5%/3 mm criteria in most cases. AAA was 2 to 3 times faster than AXB for IMRT, whereas AXB was 4–6 times faster than AAA for VMAT.

Conclusions: AXB was found to be satisfactorily accurate when compared to measurements in the RPC H&N phantom. Compared with AAA, AXB results were equal to or better than those obtained with film measurements for IMRT and VMAT plans. The AXB_ $D_{m,m}$ reporting mode was found to be closer to TLD and film measurements than was the AXB_ $D_{w,m}$ mode. AXB calculation time was found to be significantly shorter ($\times 4$) than AAA for VMAT. © 2012 American Association of Physicists in Medicine. [http://dx.doi.org/10.1118/1.3692180]

Key words: Acuros XB, deterministic method, IMRT, VMAT, RPC

I. INTRODUCTION

Modern radiation therapies such as intensity-modulated radiation therapy (IMRT) and volumetric-modulated arc therapy (VMAT) can produce highly conformal radiation dose distributions and enhance treatment localization, but these complex treatment techniques also place higher demands on dose calculation algorithms in terms of both accuracy and computation speed.^{1,2} Current dose calculation approaches can be

categorized either as pencil beam methods,³ convolution-superposition methods such as the anisotropic analytical algorithm (AAA),^{4,5} collapsed-cone convolution (CCC),⁶ and Monte Carlo (MC) methods such as EGSnrc and VMC.^{7–9} Recently, a novel deterministic method, Acuros XB, became commercially available for external photon beam dose calculations.^{10–13} The AXB fundamental radiation transport theory is based on the grid-based Boltzmann solver (GBBS), commonly known as discrete ordinates. The

linear Boltzmann transport equation (LBTE) is the governing equation that describes the distribution of radiation particles resulting from their interactions with matter. The dose for a certain volume of matter can be exactly obtained after solving for the particle fluence in the LBTE. The MC method is one approach to solving the LBTE by stochastically simulating the interacting particles, and it has been widely considered the gold standard for dose calculation accuracy in radiotherapy. Another approach to solving the LBTE is the deterministic GBBS method, which directly discretizes the energy, angle, and space variables of the LBTE into grids and iteratively solves the LBTE in discrete, multi-dimensional space. Ideally, if MC simulates an infinite number of particles and the GBBS discretizes to infinitely small steps, both methods should converge to the same solution and should have the same dose calculation accuracy.¹⁴

In 2006, Gifford *et al.*¹⁵ first validated the dose calculation from a general-purpose GBBS called Attila (Transpire, Inc., Gig Harbor, WA) for brachytherapy and external photon beam therapy. After that, several versions of the GBBS have been developed and verified in previous studies.^{10,16} In 2010, Varian Medical Systems (Palo Alto, CA) released the first version of a clinical deterministic dose algorithm in the Eclipse treatment planning system (TPS), the Acuros[®] XB (AXB) advanced dose calculation algorithm. In a previous study, we validated the performance of a preclinical version of AXB 10.0.24 in a basic slab phantom and found that the results of dose calculations from the AXB were very close to those from MC method and superior to the widely used AAA and CCC convolution methods.¹¹ Several validation studies from other groups showed similar findings.^{12,13} However, validations reported in the literature to date are mostly fundamental studies using either a simple geometric phantom or relatively simple beam setup. As the AXB algorithm moves forward to routine clinical use, where more complex IMRT or VMAT plans are common, experimental verification of this dose calculation algorithm for IMRT and VMAT planning in a simulated patient will be needed.

The motivation of this study was to experimentally verify the dosimetric performance of AXB for clinical IMRT and VMAT plans by both thermoluminescent dosimeter (TLD) and film measurements in an anthropomorphic phantom. In an attempt to keep our study more generalizable and standardized, we used the head and neck (H&N) IMRT phantom from Radiological Physics Center (RPC) since it is a well-known phantom in the medical physics community. This phantom was initially designed specifically for credentialing institutions who wanted to use IMRT to treat patients on Radiation Therapy Oncology Group (RTOG) H&N protocols and has been used in several other IMRT validation studies.^{17,18} Furthermore, by comparing AXB with the widely used AAA algorithm, we can evaluate the dosimetric impact of this new algorithm with regards to IMRT and VMAT credentialing for RTOG clinical trials. Thus, the evaluation of the AXB algorithm in this study was conducted by following the RPC H&N credentialing procedures and comparing doses calculated from AXB with (1) measured data from the RPC H&N phantom and (2) doses calculated from the existing Eclipse AAA

dose algorithm. Based on the previous studies from us and others, the AXB tends to be more accurate than AAA. Thus, at the onset of this work, we hypothesized that the measured doses would be in better agreement with doses calculated with AXB than with doses calculated with AAA.

II. MATERIALS AND METHODS

II.A. RPC H&N phantom and insert

As shown in Fig. 1(a), the RPC H&N phantom consists of a head-and-neck-shaped plastic outer shell and polystyrene inserts. The shell is a tissue-equivalent material that can be filled with water to simulate human tissue. The dosimetry insert was designed to simulate an oropharyngeal tumor [primary planning target volume (PTV)] and peripheral nodes (secondary PTV) in close proximity to an organ at risk (OAR), the spinal cord. The dosimetry insert has two halves that can be separated for the insertion and removal of dosimeters [Fig. 1(b)]. In this study, both TLDs and films were used in this dosimetry insert. Eight cavities in the insert accommodate TLD capsules to measure absolute point doses: four TLDs in the primary PTV, two TLDs in the secondary PTV, and two TLDs in the spinal cord OAR [Fig. 1(c)]. Three slots accommodate radiochromic films [GafChromic[®] EBT2, International Specialty Products (ISP), NJ] to measure the planar dose distributions in the axial and sagittal planes. One film can be inserted between the two blocks of insert in the axial plane, and two additional pieces of film can be inserted inside the blocks to form a single sagittal plane [Fig. 1(b)]. A more detailed description of the RPC H&N phantom can be found in a previous RPC publication.¹⁹

II.B. IMRT and VMAT planning and delivery

The H&N phantom was simulated with use of a Philips Brilliance 64-slice computed tomographic (CT) scanner (Philips Healthcare, Andover, MA) and the AcQSim workstation. The slice thickness was set to 1.5 mm to improve TLD visualization. The reconstructed digital imaging and communications in medicine (DICOM) CT data were imported to the Eclipse[™] TPS (Varian Medical Systems) for contouring and planning. The structures, including PTVs, OAR, and TLDs, were manually contoured. All TLD contours were set to high-resolution structures to achieve better delineation accuracy.

The prescriptions and optimization objectives used for both IMRT and VMAT treatment plans were based on the RPC phantom irradiation specifications. These objectives were modified from an RTOG H&N protocol prescription by scaling the prescription down by a factor of 10. The planning objectives were (1) at least 95% of the primary PTV must receive its prescription dose ($D_{95\%} \geq 6.6$ Gy); (2) at least 95% of the secondary PTV (STV) must receive at least 5.4 Gy ($D_{95\%} \geq 5.4$ Gy); (3) the OAR must not receive >4.5 Gy (one-tenth of the 45 Gy dose limit for the spinal cord); (4) the hot spots must be minimized; and (5) 99% of each target volume must receive more than 93% of that target's prescription

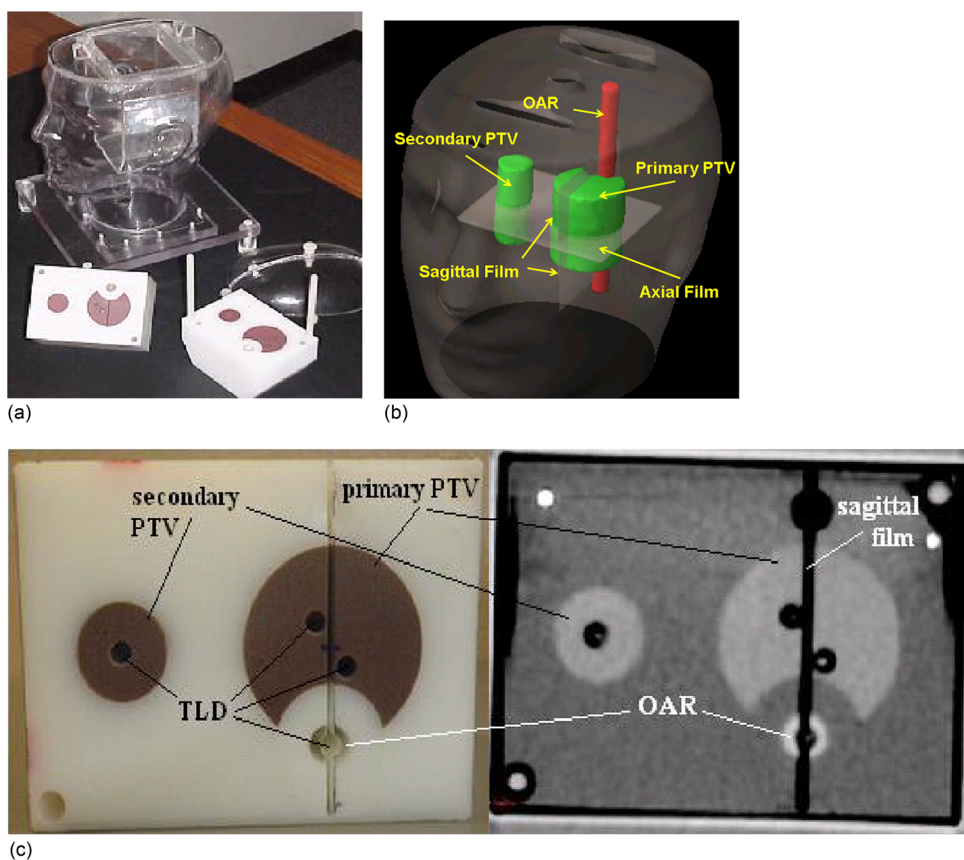


FIG. 1. RPC head and neck IMRT phantom (a) and inserts: PTV, STV, OAR, three films (b) and eight TLD capsules. The location of four TLD capsules in the upper part of the insert (c) and another set of four TLD capsules were in the corresponding location in the lower part of the insert; it also shows one axial CT slice of the inserts.

dose. The treatment couch, defined by using the Exact® couch top with flat panel structure with the rails in the out position as implemented in the Eclipse TPS, was included and set at 0° in the treatment plan.

Both IMRT and VMAT plans were generated in the Eclipse TPS 10.0. For all treatment plans, the fast superposition convolution algorithm (multiresolution dose calculation) was used for optimization. Both IMRT and VMAT plans were initially optimized until the planning criteria set by the RPC were met. More optimization attempts were made to improve the homogeneity and conformity of the dose distributions. After optimization, the dose calculations were completed using both AAA and AXB. The IMRT plan had nine coplanar, equally spaced 6-MV beams with a 0° collimator rotation. The beam angle distributions were based on the typical clinical H&N planning parameters at our institution (200°, 240°, 280°, 320°, 0°, 40°, 80°, and 160°). On average, the final IMRT beam had 102 segments (with standard variation of ± 24), in which the smallest segments is 76, and the largest segment is 141. The IMRT plan geometry is shown in Fig. 2(a). The VMAT plan had two 6-MV arcs and a collimator offset of $\pm 15^\circ$ (345° and 15°), as shown in Fig. 2(d). The final VMAT plans had 177 control points for each arc.

The planned IMRT and VMAT treatments were delivered to the RPC H&N phantom using a Varian Clinac iX linear accelerator (Varian Medical Systems) using the Mosaiq

record and verify system (IMPAC Medical Systems, Sunnyvale, CA). Treatment delivery and measurement were repeated three separate times for the IMRT and VMAT plan each, for reproducibility.

II.C. AXB and AAA dose algorithms in Eclipse TPS

AXB and AAA dose algorithms were used in the dose calculation of the IMRT and VMAT plans. Even though the Eclipse TPS designates VMAT as RapidArc, throughout this article, we use the more general term VMAT. Both algorithms were commissioned with the Varian Golden Beam data, and we reported the fundamental validation in water phantom in our previous study.¹¹ The detailed mathematical formulas and implementations including beam modeling, material assignments, and calculation options for AXB have been described in the previous publications.^{10,15} AAA and AXB share the same beam model, which was configured through the TPS beam configuration feature.

The same version of AAA (10.0.24) and a new version of AXB (11.0.03) were used in this study. Compared with the previous version, the new one had several updates: (1) improved efficiency of the algorithm by optimizing parallelization, cache usage, etc.; (2) reduced electron energy cutoff to 200 keV from 500 keV; (3) improved photon ray tracing and electron contaminant source efficiency for cases with

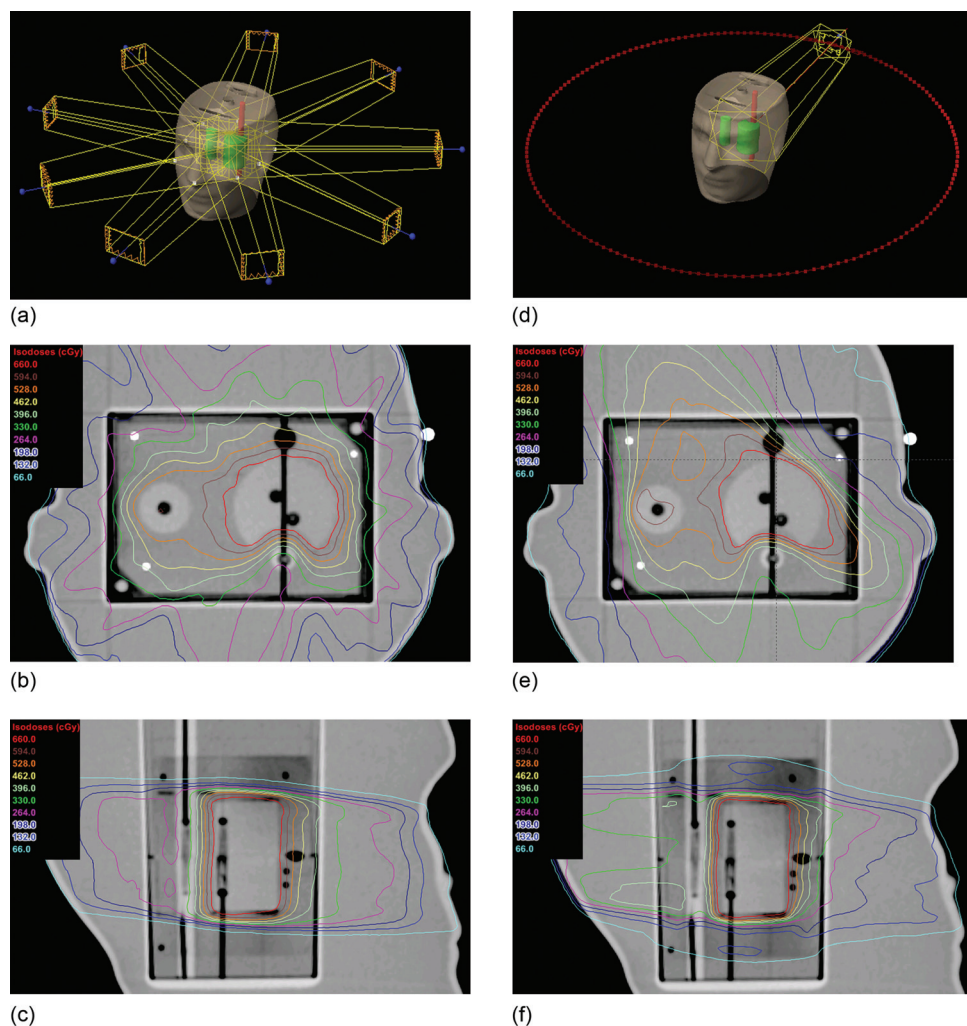


FIG. 2. IMRT (left) and VMAT (right) plan geometries [(a), (d)] and dose distributions in axial views [(b), (e)] and sagittal views [(c), (f)], which contain films.

many fields; (4) implementation of “transport correction” to accelerate iterative convergence and improve accuracy; and (5) improved handling of structure boundary when Hounsfield unit (HU) or material is assigned.

Because the AXB dose algorithm explicitly solves for radiation transport in materials, it by default reports the dose-to-medium in medium ($D_{m,m}$), which is generally referred to as dose-to-medium.¹¹ However, dose-to-water in medium ($D_{w,m}$) is more commonly used in clinical practice; thus, AXB also provides the $D_{w,m}$. The difference between these two reporting modes is only in the postprocessing step, in which the energy-dependent fluence calculated by AXB’s transport is multiplied by different flux-to-dose response functions to obtain the local absorbed dose value. These response functions depend on the macroscopic electron energy deposition cross section and the material density.²⁰ For $D_{m,m}$, the material for each voxel in the patient image is assigned according to that voxel’s CT number, and AXB uses a medium-based response function; similarly, the $D_{w,m}$ uses a water-based response function. Their differences, also called energy deposition ratios, are very similar to the

stopping power ratios used in MC methods.^{20,21} For AAA, dose is reported in only one way, and although the AAA dose is sometimes referred to as “dose to water” since its dose results are based on electron density scaled water, our previous study and other literature have indicated that AAA dose values are closer to dose-to-medium in medium.^{11,22} To avoid confusion, we refer to the dose from AAA simply as AAA dose without further differentiating it as dose-to-medium or dose-to-water.

II.D. Data analysis

The irradiated TLDs and films were read using the RPC’s standard procedures to reduce uncertainty.^{19,23} The measured TLD doses were used to compare the delivered absolute dose to the mean computed dose values inside the TLD contours. For our analysis, the irradiated films were sampled at a 0.3-mm resolution and compared with the corresponding treatment plan dose distribution. A set of three tiny pinholes in each film were used to register the film measurements and planned dose distributions within the H&N phantom.

Considering the position uncertainty of these registration holes on the films relative to their location on the CT image, we visually determined whether a net shifting (smaller than 1 mm) was required to account for this uncertainty. To reduce the noise in the film measurements, the film O.D. values were smoothed using a moving average smoothing function with 7×7 data points.

To allow a comparison with absolute dose, the film dose was normalized to the corresponding measured TLD dose in the primary or secondary PTV after correcting the film O.D. values for the film's nonlinear dose response. For example, for the axial film, the average of the superior and inferior TLD doses was used to determine the dose normalization value for the film-measured dose distribution. For each film plane measurement, axial or sagittal, we used the average of its TLD/O.D. film measurement ratios to correct the film to absolute dose.

For the planar dose comparison between measurements and calculations, two cross profiles for each film were constructed to intersect the center of the primary PTV in each orthogonal direction. The anterior-posterior and lateral profiles from the axial film and the superior-inferior profile from the sagittal films were evaluated. The measured profiles were compared with the corresponding planned dose profiles.

The measured and calculated 2D dose distributions were compared using a Gamma Index analysis²³ using a 3-mm distance-to-agreement (DTA) and 5% dose difference ($\pm 5\%/3$ mm) criteria. These criteria are used clinically at our institution for IMRT and VMAT quality assurance. The gamma analyses were repeated using a more stringent criteria of $\pm 3\%/3$ mm [IMRT commissioning standard from the American Association of Physicists in Medicine Task Group 119 (TG 119)]²⁴ and less stringent criteria of $\pm 7\%/4$ mm (RPC acceptance criteria). For all the gamma analysis criteria, a passing rate of 90% of the pixels meeting the criteria was defined as acceptable. During comparison, a mask was generated to exclude the pixels with large uncertainties: (1) below a threshold of 20% of the maximum calculated dose, (2) inside 3 mm from the edge of films, and 3) near the pinholes. All registration and gamma analyses were performed in a platform developed with MATLAB R2008b (The MathWorks, Inc., Natick, MA).

III. RESULTS

III.A. TLD results

Measured and calculated TLD doses are provided in Table I. Specifically, we reported doses from the TLD measurements and doses calculated with AAA and AXB using both dose report modes (AXB_D_{w,m} and AXB_D_{m,m}) at the corresponding locations in the phantom for the IMRT and VMAT plans. Each measurement point is identified by the position of the TLD in the phantom. The relative standard errors (RSE) of three deliveries at eight TLD capsule locations were less than 1% for most of the measurement locations and were all within 2%, indicating little variation in TLD measurements across IMRT and VMAT treatment deliveries. Compared with TLD measured doses, the calcu-

TABLE I. The comparison between TLD measurements and the dose calculations from AAA and AXB (D_{w,m} and D_{m,m}).

TLD position	Measurements		$(\Delta\%)^a$		
	Average (cGy)	RSE (%)	AAA	AXB D _{w,m}	AXB D _{m,m}
(a) IMRT plan					
PTV_I_ant ^b	707.7	0.48	0.47	2.07	0.77
PTV_S_ant	711.8	0.41	1.19	1.93	0.77
PTV_I_post	709.1	0.73	0.37	1.22	0.16
PTV_S_post	715.3	0.49	1.56	0.43	1.41
STV_I	593.1	0.87	0.33	1.77	0.29
STV_S	595.5	0.89	0.28	1.09	0.79
OAR_I	298.3	1.5	4.51	2.29	1.49
OAR_S	300.1	1.82	3.43	2.23	1.53
Average $\Delta\%$			1.52	1.63	0.90
(b) VMAT plan					
PTV_I_ant	741.1	0.68	4.65	5.88	4.64
PTV_S_ant	743.6	1.08	1.81	2.66	1.51
PTV_I_post	732.4	1.01	2.07	3.23	1.9
PTV_S_post	733.4	0.71	1.11	2.47	0.68
STV_I	621.6	0.04	1.56	3.02	1.56
STV_S	600.9	1.45	0.68	1.86	0.01
OAR_I	359.4	1.01	0.35	4.04	2.24
OAR_S	357.4	0.06	1.25	5.92	3.17
Average $\Delta\%$			1.69	3.64	1.96

^a $\Delta\% = 100 \times \text{abs}(D_{xxx} - D_{TLD})/D_{TLD}$; RSE = (std/mean) of measurements $\times 100$.

^bThe TLD position is described by the structure where it is located (PTV, STV, or OAR) and its placement within that structure [superior (S) versus inferior (I) and, when applicable, anterior (ant) versus posterior (post)].

lated dose values within the two PTV's from AAA and AXB_D_{m,m} are mostly within 5% for all six point doses, and the average percentage difference is within 2%. The measured and calculated doses in the OAR, where the dose delivered was much less and possible dose gradients exist, were within 5%. There was no appreciable difference in the dose comparisons between the IMRT and VMAT deliveries except the VMAT disagreements were slightly larger (average percent differences of 1.5%, 1.6%, and 0.9% for IMRT versus 1.7%, 3.6%, and 2.0% for VMAT). Calculated dose values from AXB_D_{w,m} have relatively worse agreement with TLD measured doses; nevertheless, differences are still within 6%, and the averages of percentage differences are within 4% when looking at both IMRT and VMAT deliveries.

III.B. Film results

Measured and calculated (AAA and AXB) film doses are compared in Fig. 3. IMRT dose profiles are shown in Figs. 3(a)-3(c), and VMAT dose profiles are in Figs. 3(d)-3(f). Data shown in Fig. 3 are for the first delivery of the VMAT and IMRT plans, similar results were observed for the second and third irradiations. In general, the profiles from AXB agreed well with those from the films. The AAA dose values were somewhat higher than those from film and

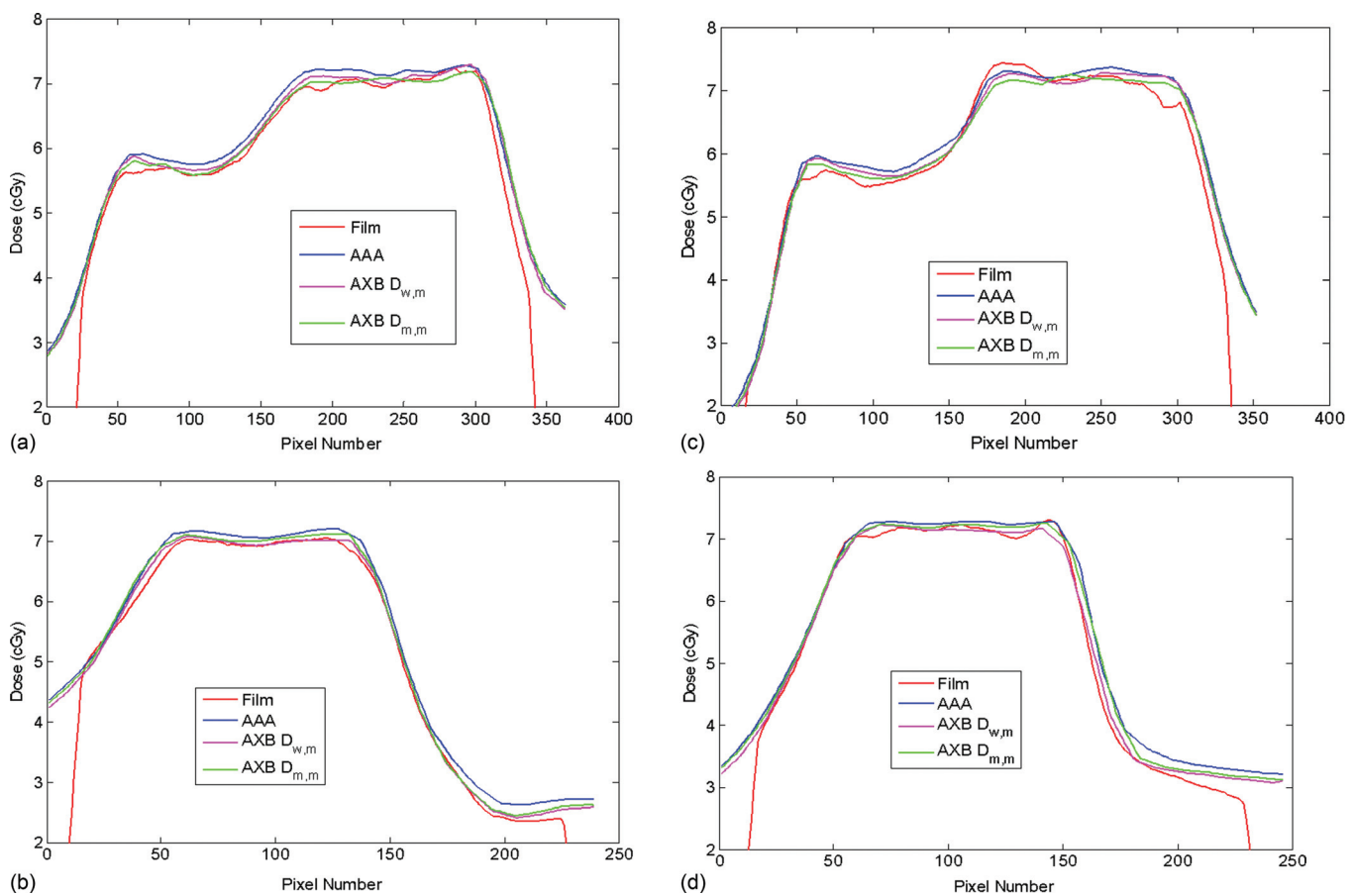


FIG. 3. Comparison of dose profiles for AAA, AXB, and film measurement in the IMRT (a)-(b) and VMAT (c)-(d) plan. The profiles are for the lateral and anterior-posterior lines marked in Fig. 2.

AXB. From the profile comparison, we can observe that the displacements of the measured penumbra are all within 1.5 mm DTA in all cases (passed the RPC 4 mm DTA criteria), which are all in good agreement to the planning.

III.C. Gamma analysis results

Figure 4 shows the spatial distribution of the gamma analyses with $\pm 5\%/3$ mm criteria for the first delivery of the VMAT and IMRT plans, and similar results were observed for the second and third irradiations. From these data, we observed that (1) the difference between measured film doses and those calculated with AXB_D_{m,m} and AXB_D_{w,m} were relatively small; and (2) the areas of dose differences between measured and calculated doses were somewhat larger when doses were calculated with AAA rather than with AXB. Furthermore, we found that agreement between measured and calculated film doses was worse for VMAT plans than for IMRT plans. The percentage of pixels that passed the gamma index criteria of $\pm 5\%/3$ mm are provided in Table II. For both IMRT and VMAT, more than 88% of the pixels passed the $\pm 5\%/3$ mm criteria for AXB (D_{m,m} and D_{w,m}), but the AAA had only an 80%–85% passing rate. Similar to the qualitative findings observed in Fig. 4, VMAT agreement was somewhat worse than IMRT agreement for both AAA and AXB.

To further study the tolerance of dose difference to the passing rate, we increased the restriction of gamma criteria to $\pm 3\%/3$ mm and released it to $\pm 7\%/4$ mm. The mean percents of voxels passing the gamma analyses for all plans (IMRT and VMAT) were plotted for AAA and AXB (D_{m,m} and D_{w,m}) as a function of gamma criteria in Fig. 5. As expected, we observed that with less stringent criteria, the percentage of passing pixels increased for all dose calculation methods. For AXB (D_{m,m} and D_{w,m}), most of the IMRT and VMAT plans passed the $\pm 5\%/3$ mm criteria, and some of the IMRT plans passed the $\pm 4\%/3$ mm criteria. However, for AAA, most plans passed at only the least stringent criterion level, $\pm 7\%/4$ mm.

III.D. Dose volume histogram (DVH) comparison between AXB and AAA

Figure 6 compares DVHs from the IMRT and VMAT plans calculated with AAA and AXB. The DVHs were shown to be very similar for normal tissue structures, but some notable differences in PTVs (primary and secondary) and significant differences in OAR structures were observed. Table III shows a more detailed quantitative analysis of the DVH comparison. The percent differences in mean dose between AXB and AAA were within 2% in normal tissue, 5% in PTVs, and 7.5% in OAR structures. The differences

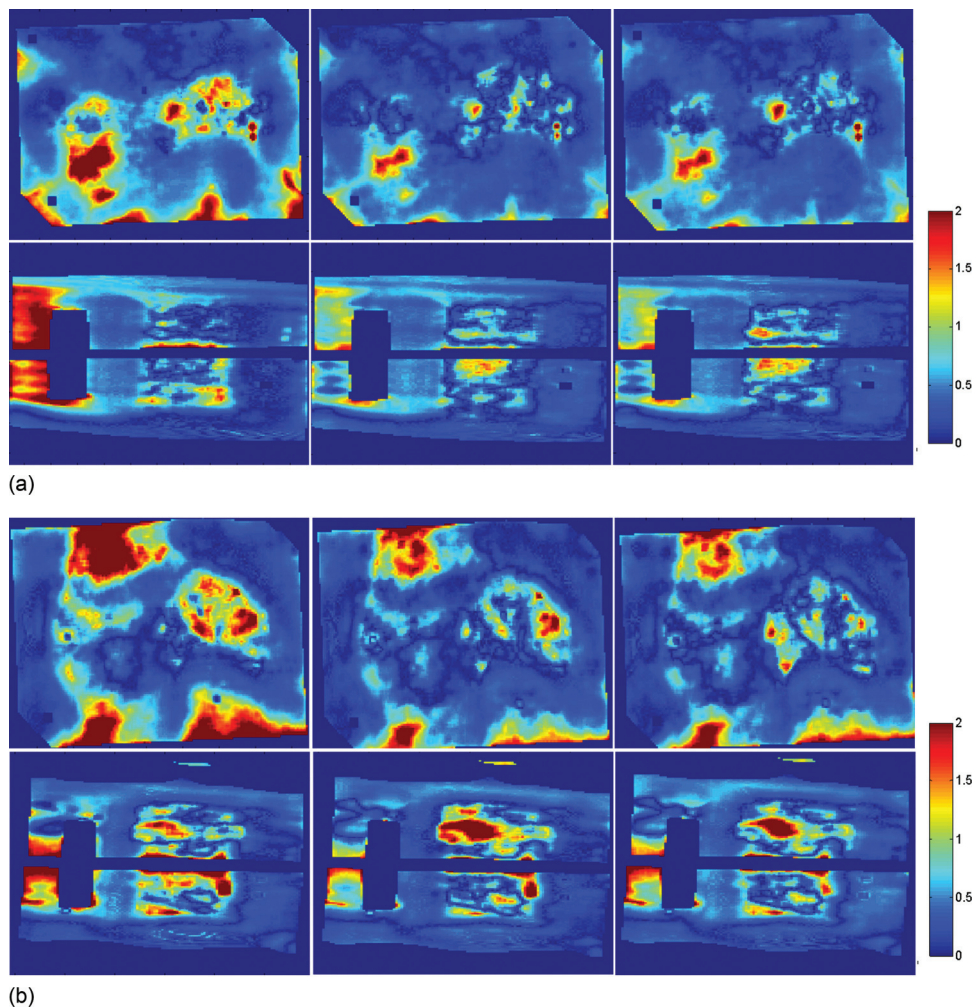


FIG. 4. The distribution of gamma index with a $\pm 5\%/3$ mm criteria for the first delivery (axial on the top, sagittal on the bottom) for IMRT (a) and VMAT plans (b). From left to right, the results are for AAA, AXB_{D_{w,m}}, and AXB_{D_{m,m}}, respectively.

between the AAA and AXB DVHs of the IMRT plan were larger than those between the AAA and AXB DVHs of the VMAT plan.

III.E. Computation time

The Eclipse TPS used in this study, which includes both the AXB and AAA algorithms, was installed on a standard clinical workstation (Dell T5500) with dual 2.27-GHz quad-core Intel processors E5520, 24-GB RAM memory, and a 64-bit Windows XP operating system. The real computation times for the IMRT and VMAT plans are listed in Table IV.

TABLE II. Mean percentage of points passing gamma analysis for $\pm 5\%/3$ mm criteria. Standard deviations (in parentheses) and mean values were calculated from three deliveries.

Film position	AAA	AXB _{D_{w,m}}	AXB _{D_{m,m}}
IMRT_axial	82.7 (2.7)	92.7 (1.7)	91.6 (1.6)
IMRT_sagittal	85.1 (2.2)	95.2 (1.3)	95.3 (1.2)
VMAT_axial	79.5 (3.4)	88.9 (1.0)	89.2 (1.1)
VMAT_sagittal	84.8 (2.8)	90.0 (0.7)	91.1 (0.9)

The AAA and AXB computation times were comparable for the IMRT plan, but the AXB time was about 4 times faster than the AAA time for the VMAT plan.

IV. DISCUSSION

In this study, we experimentally verified the dosimetric performance of AXB for complex clinical treatment plans, i.e., IMRT and VMAT in an anthropomorphic H&N phantom. The dosimetric performance was verified by comparing AXB calculated treatment plans with TLD and film measurements and with plans calculated using the standard AAA method in the Eclipse TPS. The results showed that the dose agreement of AXB_{D_{m,m}} was within 5% of doses measured with TLD for all measurement points and that gamma analysis of the film measurements passed the $\pm 5\%/3$ mm criteria (90% passing rate). Compared with AAA, the AXB_{D_{m,m}} had equivalent agreement to TLD data and better agreement with the film measurements. With AXB, the gamma passing rate of RPC would improve about 10% over AAA. We also compared the two AXB dose reporting modes, D_{m,m} and D_{w,m}, with TLD and film measurements. Our results showed

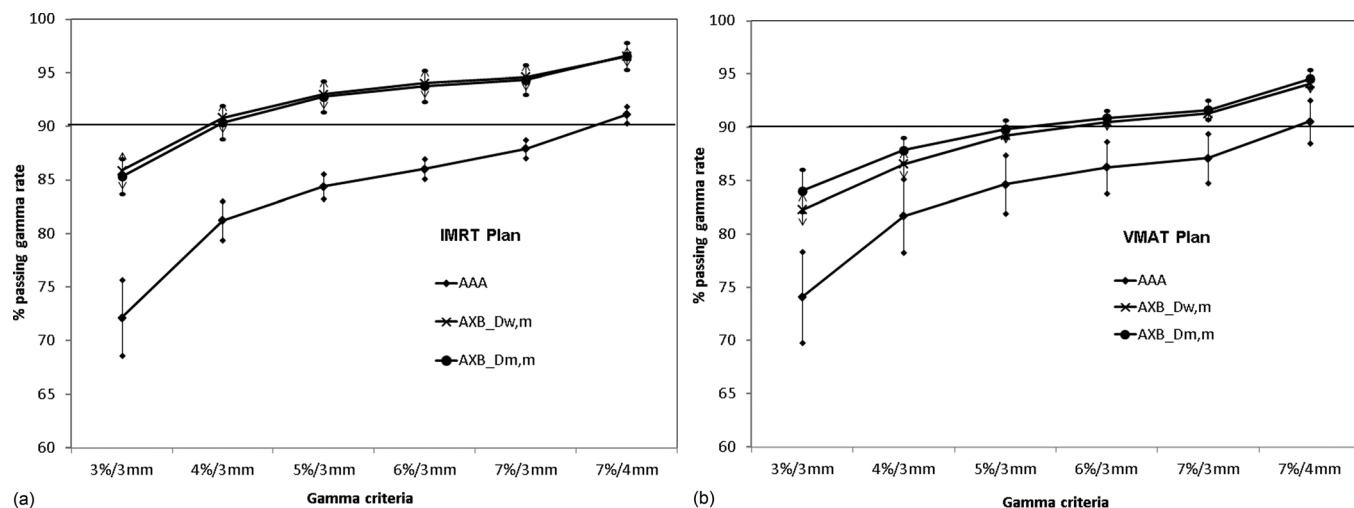


FIG. 5. Percentage of voxels passing gamma analysis with various criteria (from $\pm 3\%$ /3 mm to $\pm 7\%$ /4 mm).

that the AXB_{D_{m,m}} data were closer to TLD data than the AXB_{D_{w,m}} data were to TLD data and that their dose distributions were similar to those of film measurements. A comparison of DVHs from AAA and AXB showed that the differences in mean dose in normal tissue (within 2%) and in PTV structures (within 5%) were in acceptable agreement, but larger differences (4.5%–7.3%) in OAR structures were found, indicating that there are still notable differences for AAA and AXB dose calculations.

The film gamma analysis from both AAA and AXB in this study passed the RPC gamma criteria (7%/4 mm) but did not pass the more stringent 3%/3 mm criteria recommended by TG 119. However, it is important to note that the RPC standard credentialing procedure for both treatment planning and measurements is very different from the procedure described in TG 119. First, the RPC procedure uses a head shaped phantom rather than a phantom with a flat surface. Second, the RPC procedure uses TLD as an absolute dosimeter rather than an ion chamber. Third, the RPC procedure uses absolute dose Gamma analysis rather than relative dose analysis. Finally, the RPC procedure uses a film registration method with larger uncertainty than precise integrated device film registration recommended by TG 119.

Using the RPC H&N phantom for the purpose of investigating dosimetric performance of AXB has both advantages and disadvantages. One advantage was that this phantom was designed for the specific purpose of credentialing institutions participating in RTOG H&N protocols involving IMRT and has been used in several other IMRT validation studies. Thus, this is a highly standardized method and has been used for many other validation studies.^{17,25} The results showed that the passing rate of AXB was better than that of AAA, indicating that a better dose algorithm might also improve the credentialing test passing rate by reducing the uncertainty introduced by dose algorithm. However, there are some limitations associated with the use of this phantom for algorithm validation. The RPC H&N phantom is made primarily from water-equivalent materials. Although there are air gaps near the TLD and film insert gaps, these air gaps

are very small and their effects to the dose calculation are negligible. Thus, the effects from heterogeneities expected in a clinical treatment could not be fully investigated. Based on our previous comparison study using a heterogeneous slab phantom¹¹ and on other studies,^{12,13} the dose differences between AAA and AXB might be up to 15% in the lung region, especially for smaller field sizes. Thus, the experimental comparison between AAA and AXB for smaller field sizes, such as those seen in stereotactic body radiotherapy (SBRT) using a more heterogeneous phantom, will be an interesting topic for the further studies.

In this study, the DVHs from AAA and AXB (Fig. 6) were similar (over most regions), and the greatest mean dose differences (7.3%) were found within the cord OAR tissue (with a maximum dose difference of 3.7%). Similar findings were also reported for comparisons with AAA with Monte Carlo.²⁶ Although it does not impose a significant clinical impact in translating between AAA and AXB, the results show the potential benefits of improved dose algorithm. Considering that the RPC H&N phantom are largely water equivalent, the dose differences between AAA and AXB are mostly attribute to the scatter component of dose calculation in which AXB directly solve the radiation transport while AAA apply a density-related scatter kernel. For this study, the AAA dose results were generally higher than AXB and overestimated to film. However, more generally, AAA might also underestimate dose depending on the beam energy, field sizes, and tissue materials based on our previous studies.¹¹

The comparison between D_{m,m} and D_{w,m} in this study gives some useful insights on which dose reporting mode should be used when comparing calculated dose with TLD and film measurements. More generally, it has been debated whether the MC dose predictions need to be converted to D_{w,m} when comparing with TLD measurements.^{21,27,28} Similar to MC methods, the AXB algorithm solves the radiation transport problem in specific material and by default reports D_{m,m}. The results from this study indicate that the D_{m,m} dose values from AXB or MC might not need to be converted to D_{w,m} when comparing with TLD measurements. First, the dose results

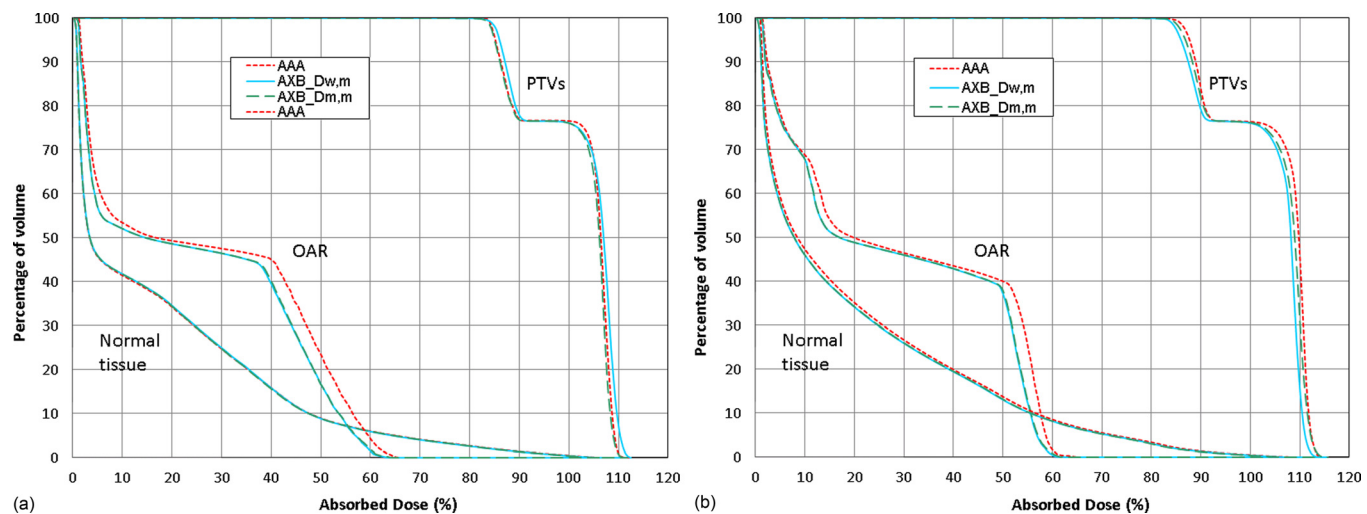


FIG. 6. Comparison of DVHs calculated by AAA, AXB_{D_{w,m}}, and AXB_{D_{m,m}} for IMRT (a) and VMAT (b) plan.

from D_{m,m} are more close to TLD and film data than D_{w,m}. Second, the dose results from D_{m,m} are more close to other widely used algorithms (AAA in this study) than D_{w,m}, which is also consistent with our previous studies and those of other groups (both AAA and CCC).^{11,29} Thus, the D_{m,m} might be the final dose value that the TPS needs to provide clinically.

Generally, the differences between D_{m,m} and D_{w,m} are very small for those regions with water or water-equivalent tissues but become larger for air cavities and bone tissue due to the large differences of water-to-air and water-to-bone energy deposition ratios. Previous studies have shown that their differences may be as high as 15% for bone tissue.^{21,28} In this study, since the RPC HN phantom do not have any bone tissue, the major differences between AXB_{D_{w,m}} and AXB_{D_{m,m}} should be located near the air regions and penumbra regions. Our results were consistent with this hypothesis. The film gamma analyses in Figs. 4 and 5 showed that the gamma map and the gamma passing curves of AXB_{D_{w,m}} and AXB_{D_{m,m}} are very close, which is attributed to the film being water-equivalent. On the other hand, the TLD measurement comparison in Table I showed large differences between the absolute dose values calculated with

AXB_{D_{w,m}} and AXB_{D_{m,m}}, which is attributed to the TLDs being surrounded by air gaps. Since the AXB_{D_{w,m}} uses the water-based response function in the air cavity, the dose value tends to be underestimated. This result also suggests that the air gap should be minimized to achieve better agreement with TLD measurements.

In this study, the IMRT measurements were in better agreement with their corresponding calculations than the VMAT measurements and their corresponding calculations. This may be attributed to the higher complexity of the VMAT plan. In order to deliver the degree of modulation of dose necessary for more complex plans, the IMRT plan would only need to increase the MU and number of segments at a static gantry angle, while the VMAT can vary these factors as well as the gantry rotation speed. Although the MLC deviations did not seem to vary between VMAT treatments, the additional uncertainty of the gantry position, gantry rotation speed, and MLC positions are compounded in VMAT treatments and could be the cause of the differences in the dose delivery from treatment to treatment. The effects of these complex motions and their uncertainties need to be fully understood for QA and should be further investigated.

The computation time of the AXB dose algorithm in VMAT planning was significantly reduced compared with that of the AAA. This is due to the fact that AXB only calculates the primary source (uncollided) component for each beam via ray-tracing, whereas the scatter components can be calculated only once regardless of the number of beam angles by resolving the LBTE.²⁰ Thus, in the case of VMAT plan in which each beam have a large number of orientations, the AXB can reduce the total computation time largely. With the increasing interest in VMAT for various

TABLE III. Mean dose differences from DVHs of plans calculated by AAA and AXB. Dose differences were relative to AAA dose value. Values for both IMRT and VMAT plans are listed.

	Mean dose(cGy)			$\Delta\%$ _AAA ^a	
	AAA	AXB _{D_{m,m}}	AXB _{D_{w,m}}	AXB _{D_{m,m}}	AXB _{D_{w,m}}
IMRT plan					
PTVs	685.6	672.1	677.9	4.8	4.7
OAR	119.8	114.0	114.2	7.1	7.3
Normal tissue	174.7	162.3	161.9	2.0	1.1
VMAT plan					
PTVs	693.5	683.1	689.0	3.4	3.1
OAR	133.5	128.9	129.3	4.6	4.8
Normal tissue	195.5	186.6	186.1	1.5	0.6

^a $\Delta\%$ _AAA = 100 × abs(D_{xxx} - D_{AAA})/D_{AAA}.

TABLE IV. Computation times (in minutes) of AAA and AXB for IMRT and VMAT plans.

	AAA	AXB _{D_{w,m}}	AXB _{D_{m,m}}
IMRT	2.3 (0.1)	3.1 (0.1)	3.1 (0.1)
VMAT	16.0 (1.2)	4.2 (0.3)	4.3 (0.3)

clinical applications, AXB could provide both accuracy and fast computation speed for treatment planning.

V. CONCLUSIONS

The introduction of the novel deterministic AXB algorithm in the Eclipse TPS provides a new option for improving accuracy and efficiency in the clinical practice of radiotherapy. The experimental validation study using the RPC IMRT H&N phantom showed that AXB is satisfactorily accurate and provides equivalent or better agreement to both TLD and films than AAA. AXB decreases computation time over AAA on the order of four for VMAT planning.

ACKNOWLEDGMENTS

This work was funded by National Institutes of Health Grant No. 2R44CA105806-02 and CA010953 and MD Anderson's Cancer Center Support Grant No. CA016672. The authors thank Stephen K. Thompson, Pekka Uusitalo, Laura Korhonen, and Tuomas Torsti from Varian Medical Systems and Gregory A. Failla, Todd A. Wareing, and John McGhee from Transpire, Inc., for providing the prototype version of the Eclipse system. They also thank Andrea Molineu from the Radiological Physics Center at The University of Texas MD Anderson Cancer Center for help in RPC measurements and valuable discussions.

- ^aAuthor to whom correspondence should be addressed. Electronic mail: rhowell@mdanderson.org
- ¹B. Vanderstraeten, N. Reynaert, L. Paelinck, I. Madani, C. De Wagter, W. Gersem, W. De Neve, and H. Thierens, "Accuracy of patient dose calculation for lung IMRT: A comparison of Monte Carlo, convolution/superposition, and pencil beam computations," *Med. Phys.* **33**, 3149–3158 (2006).
 - ²K. Otto, "Volumetric modulated arc therapy: IMRT in a single gantry arc," *Med. Phys.* **35**, 310–317 (2008).
 - ³A. Ahnesjo, M. Saxner, and A. Trepp, "A pencil beam model for photon dose calculation," *Med. Phys.* **19**, 263–273 (1992).
 - ⁴A. Fogliata, G. Nicolini, E. Vanetti, A. Clivio, and L. Cozzi, "Dosimetric validation of the anisotropic analytical algorithm for photon dose calculation: Fundamental characterization in water," *Phys. Med. Biol.* **51**, 1421–1438 (2006).
 - ⁵B. Murray, C. Newcomb, K. Breitman, S. Connors, P. Dunscombe, G. Field, M. MacKenzie, S. Rathee, D. Robinson, H. Warkentin, and B. Fallon, "Experimental validation of the Eclipse AAA algorithm," *Med. Phys.* **33**, 2661–2661 (2006).
 - ⁶A. Ahnesjo, "Collapsed cone convolution of radiant energy for photon dose calculation in heterogeneous media," *Med. Phys.* **16**, 577–592 (1989).
 - ⁷D. W. O. Rogers, B. A. Faddegon, G. X. Ding, C. M. Ma, J. We, and T. R. Mackie, "BEAM: A Monte Carlo code to simulate radiotherapy treatment units," *Med. Phys.* **22**, 503–524 (1995).
 - ⁸I. Kawrakow, M. Fippel, and K. Friedrich, "3D electron dose calculation using a Voxel based Monte Carlo algorithm (VMC)," *Med. Phys.* **23**, 445–457 (1996).
 - ⁹C. M. Ma, E. Mok, A. Kapur, T. Pawlicki, D. Findley, S. Brain, K. Forster, and A. L. Boyer, "Clinical implementation of a Monte Carlo treatment planning system," *Med. Phys.* **26**, 2133–2143 (1999).
 - ¹⁰O. N. Vassiliev, T. A. Wareing, J. McGhee, G. Failla, M. R. Salehpour, and F. Mourtada, "Validation of a new grid-based Boltzmann equation solver for dose calculation in radiotherapy with photon beams," *Phys. Med. Biol.* **55**, 581–598 (2010).
 - ¹¹T. Han, J. K. Mikell, M. Salehpour, and F. Mourtada, "Dosimetric comparison of Acuros XB deterministic radiation transport method with Monte Carlo and model-based convolution methods in heterogeneous media," *Med. Phys.* **38**, 2651–2664 (2011).

- ¹²K. Bush, I. M. Gagne, S. Zavgorodni, W. Ansbacher, and W. Beckham, "Dosimetric validation of Acuros (R) XB with Monte Carlo methods for photon dose calculations," *Med. Phys.* **38**, 2208–2221 (2011).
- ¹³A. Fogliata, G. Nicolini, A. Clivio, E. Vanetti, P. Mancosu, and L. Cozzi, "Dosimetric validation of the Acuros XB Advanced Dose Calculation algorithm: Fundamental characterization in water," *Phys. Med. Biol.* **56**, 1879–1904 (2011).
- ¹⁴C. Borgers, "Complexity of Monte Carlo and deterministic dose-calculation methods," *Phys. Med. Biol.* **43**, 517–528 (1998).
- ¹⁵K. A. Gifford, J. L. Horton, T. A. Wareing, G. Failla, and F. Mourtada, "Comparison of a finite-element multigroup discrete-ordinates code with Monte Carlo for radiotherapy calculations," *Phys. Med. Biol.* **51**, 2253–2265 (2006).
- ¹⁶K. A. Gifford, M. J. Price, J. L. Horton, T. A. Wareing, and F. Mourtada, "Optimization of deterministic transport parameters for the calculation of the dose distribution around a high dose-rate Ir-192 brachytherapy source," *Med. Phys.* **35**, 2279–2285 (2008).
- ¹⁷P. Cadman, R. Bassalow, N. P. S. Sidhu, G. Ibbott, and A. Nelson, "Dosimetric considerations for validation of a sequential IMRT process with a commercial treatment planning system," *Phys. Med. Biol.* **47**, 3001–3010 (2002).
- ¹⁸S. Babic, J. Battista, and K. Jordan, "Three-dimensional dose verification for intensity-modulated radiation therapy in the radiological physics centre head-and-neck phantom using optical computed tomography scans of ferrous xylenol-orange gel dosimeters," *Int. J. Radiat. Oncol., Biol., Phys.* **70**, 1281–1291 (2008).
- ¹⁹A. Molineu, D. S. Followill, P. A. Balter, W. F. Hanson, M. T. Gillin, M. S. Huq, A. Eisbruch, and G. S. Ibbott, "Design and implementation of an anthropomorphic quality assurance phantom for intensity-modulated radiation therapy for the radiation therapy oncology group," *Int. J. Radiat. Oncol., Biol., Phys.* **63**, 577–583 (2005).
- ²⁰G. A. Failla, T. Wareing, Y. Archambault, and S. Thompson, *AcurosXB Advanced Dose Calculation for the Eclipse Treatment Planning System* (Varian Medical System, Palo Alto, CA, 2010).
- ²¹J. V. Siebers, P. J. Keall, A. E. Nahum, and R. Mohan, "Converting absorbed dose to medium to absorbed dose to water for Monte Carlo based photon beam dose calculations," *Phys. Med. Biol.* **45**, 983–995 (2000).
- ²²A. Fogliata, E. Vanetti, D. Albers, C. Brink, A. Clivio, T. Knoos, G. Nicolini, and L. Cozzi, "On the dosimetric behaviour of photon dose calculation algorithms in the presence of simple geometric heterogeneities: Comparison with Monte Carlo calculations," *Phys. Med. Biol.* **52**, 1363–1385 (2007).
- ²³A. Niroomand-Rad, C. R. Blackwell, B. M. Coursey, K. P. Gall, J. M. Galvin, W. L. McLaughlin, A. S. Meigooni, R. Nath, J. E. Rodgers, and C. G. Soares, "Radiochromic film dosimetry: Recommendations of AAPM Radiation Therapy Committee Task Group 55," *Med. Phys.* **25**, 2093–2115 (1998).
- ²⁴G. A. Ezzell, J. W. Burmeister, N. Dogan, T. J. LoSasso, J. G. Mechala-kos, D. Mihailidis, A. Molineu, J. R. Palta, C. R. Ramsey, B. J. Salter, J. Shi, P. Xia, N. J. Yue, and Y. Xiao, "IMRT commissioning: Multiple institution planning and dosimetry comparisons, a report from AAPM Task Group 119," *Med. Phys.* **36**, 5359–5373 (2009).
- ²⁵H. Sakhalkar, D. Sterling, J. Adamovics, G. Ibbott, and M. Oldham, "Investigation of the feasibility of relative 3D dosimetry in the Radiologic Physics Center Head and Neck IMRT phantom using Presage/optical-CT," *Med. Phys.* **36**, 3371–3377 (2009).
- ²⁶K. Bush, S. Zavgorodni, I. Gagne, R. Townson, W. Ansbacher, and W. Beckham, "Monte Carlo evaluation of RapidArc (TM) oropharynx treatment planning strategies for sparing of midline structures," *Phys. Med. Biol.* **55**, 4465–4479 (2010).
- ²⁷E. Gil, B. Clark, and J. E. Cygler, "Evaluation of dosimetric differences between dose-to-water and dose-to-medium for head and neck patients treated with electron beams," *Med. Phys.* **36**, 4318–4318 (2009).
- ²⁸B. R. B. Walters, R. Kramer, and I. Kawrakow, "Dose to medium versus dose to water as an estimator of dose to sensitive skeletal tissue," *Phys. Med. Biol.* **55**, 4535–4546 (2010).
- ²⁹E. Sterpin, M. Tomsej, B. De Smedt, N. Reynaert, and S. Vynckier, "Monte Carlo evaluation of the AAA treatment planning algorithm in a heterogeneous multilayer phantom and IMRT clinical treatments for an Elekta SL25 linear accelerator," *Med. Phys.* **34**, 1665–1677 (2007).